CrossMark

The preparation of PZS-OH/CNT composite and its adsorption of U(VI) in aqueous solutions

Yan Liu[1,2] · Ying Dai[2] · Dingzhong Yuan[2] · Yun Wang[2] · Lixia Zou[2]

Abstract In this paper, polycyclotriphosphazene coated carbon nanotubes (PZS-OH/CNT) composite material has been synthesized via a facial method. The prepared PZS-OH/CNT was characterized by FTIR, BET, zeta potential and SEM. The material was investigated as an adsorbent for the adsorption towards U(VI) from aqueous solutions. Several parameters like solution pH, contact time and temperature were used to evaluate the sorption efficiency. The results indicated that the adsorption capacity of uranium on PZS-OH/CNT was improved from 41.48 mg g^{-1} for CNT to 338.98 mg g^{-1} due to the presence of functional groups on PZS-OH/CNT. The U(VI) sorption on PZS-OH/CNT was well fitted to the Langmuir adsorption isotherm and pseudo-second kinetics models. The thermodynamic parameters (ΔH, ΔS and ΔG) showed the U(VI) adsorption on CNT and PZS-OH/CNT was endothermic and spontaneous in nature.

Keywords Polyphosphazene · Carbon nanotubes · Uranium · Adsorption

✉ Yan Liu
fzliuyan1986@163.com

1 Key Laboratory for Radioactive Geology and Exploration Technology, Fundamental Science for National Defense, East China University of Technology, Nanchang, Jiangxi 330013, China

2 School of Chemistry, Biology and Material Science, East China University of Technology, Nanchang, Jiangxi 330013, China

Introduction

Uranium contamination in groundwater is a critical issue associated with the mining, milling and processing of materials for the nuclear power industry [1]. This may not only result in wastage of limited resources, and is also harmful to the environment and associated herbal growth, so it is necessary to remove and recycle the metal ions from waste water [2]. There are various technologies explored for the removal of uranium from aqueous medium including solvent extraction, precipitation, coagulation, membrane filtration, adsorption [3–6]. Among these methods, adsorption is considered to be an efficient and promising method and the results indicated that the adsorption of U(VI) ions was mostly dominated by ion-exchange and/or surface complexation at acidic pH values [7].

A promising adsorbent suitable for use in extreme environments, such as high temperature, high radiation damage rate and aggressive chemical environments, might be carbon materials because of their excellent properties such as thermal and chemical stability [8]. Recent years, attention has been paid to the use of carbon nanotubes (CNTs), as a high capacity adsorbent material due to their large specific surface area, hollow and porous structures along with high mechanical, chemical and thermal stability. [9]. However, the limited amount of functional groups on CNTs are not enough to effectively remove U(VI) ions from aqueous solutions and the tendency of stacking of CNTs in water due to high van der waals interaction forces lowers its specific surface area. Therefore, decoration of CNTs by introducing organic and inorganic groups or particles is an effective way to enhance its dispersibility and performance [10]. Hence, further study is essential to find a simple method to modify CNTs surface by

Springer

introducing versatile functional groups to facilitate electrostatic interactions between CNTs and heavy metal ions for improving its separation performance while maintaining other excellent property [11].

Recently, cyclotriphosphazene has been the center of interest for many researchers. Cyclotriphosphazene consists of six-membered rings structures of alternating phosphorus and nitrogen atoms and has the capability of binding to metal ions via its phosphazene ring nitrogen [12]. The halogen atoms bound by phosphorus atoms in their structure may easily produce a substitution reaction with nucleophilic substances such as amines, alcohols and phenols [13]. Also, cyclotriphosphazene derivatives and macromolecules show high chemical and thermal stabilities and display various properties suitable for a wide range of applications depending on the nature of their side groups [14, 15]. Hence, it is of interest to suitably modify CNTs with cyclotriphosphazene for the adsorption of radionuclides. The material may have many advantages, such as avoid aggregation, improving the adsorption ability. Notably, the decoration of CNTs surfaces with cyclotriphosphazene has never been explored for removing uranium from aqueous environment.

In this work, we combined the polycyclotriphosphazene and CNT together to form composites via a facile and environmentally friendly method by utilizing both merits of CNTs (high surface area) and cyclotriphosphazene (abundant functional groups). The composites were used for the removal of UO_2^{2+} from wastewater. As expected, the composites exhibited higher adsorption capacity than CNTs, indicating the composites as an outstanding material to remove UO_2^{2+} efficiently. Several parameters like solution pH, contact time, initial concentrations and temperature are investigated in order to evaluate the sorption efficiency. In addition, adsorption mechanisms including adsorption kinetics, isotherm models, and thermodynamics were also analyzed.

Experimental

Materials

Multiwall carbon nanotubes (CNT, outer diameter, 10–20 nm, length, 10–30 μm, purity, > 95%) were purchased from Chengdu Organic Chemicals Co., Ltd. Hexachlorocyclotriphosphazene (HCCP), 4, 4'-sulfonyldiphenol (DOS) were provided by Aldrich Chemical Co. Ltd. Triethylamine (TEA) and other reagents were provided by Sinopharm Chemical Reagent Co., Ltd. (China). HCCP was recrystallized from hexane twice before use. Other chemicals were of analytical reagent grade without further purification.

Preparation of PZS-OH/CNT composite

The preparation of PZS-OH/CNT requires only mild conditions, just room temperature and ultrasound. The synthesized method for the composite was as follows according to the Ref. [16]: 5 mg CNT was dissolved into 80 mL of a mixed solvent of THF and ethanol (20:1 volume) and dispersed upon ultrasound (100 W, 40 kHz) for 30 min. 20 mg HCCP, 45 mg DOS and 2 mL acid-binding agent TEA were added into the above solution and maintained in the ultrasonic bath for 5 h. The resulting product was precipitated and washed with THF and deionized water, dried at 80 °C in vacuum oven (The synthesis route is illustrated in Scheme 1).

Characterization

The FT-IR spectra were recorded on a Nicolet Nexus iS5 (USA) Fourier transform infrared spectrometer in the wave number range from 4000 to 400 cm^{-1}. Surface morphology was observed by a JEOL JSM-5900 scanning electron microscopy (SEM). X-ray photoelectron spectra (XPS) were recorded on a kratos Axis Ultra DLD, and the C_{1s} line at 284.8 eV was used as a reference. Spectrophotometric analysis was carried out by UV–vis spectrophotometer (757CRT, Tianjin Guanze Technol. Co., Ltd). N_2 adsorption/desorption isotherms were measured using a Micromeritics Gaobo, (JW-BK12F, Beijing) instrument. The specific surface areas were calculated using the Brunauer–Emmett–Teller (BET) method. The zeta potential was measured using a Particle Metrix flowing current potential analyzer (Microtrac, America).

Batch and kinetic adsorption experiments

The uranium solutions were prepared by diluting the stock solution to appropriate volumes depending upon the experimental requirements. In a typical experiment, 0.01 g composite was contacted with 100 mL U(VI) solution of given pH value (adjusted by 0.1 mol L^{-1} HCl and NaOH solution), concentration and temperature. After shaking for specified durations, the suspensions were centrifuged and the concentrations of the final solutions were determined by arsenazo-III spectrophotometry method [17] by spectrophotometer at 660 nm. The amounts of adsorbed (q_e, mg g^{-1}) uranium were calculated by Eq. (1):

$$q_e = \frac{(C_0 - C_e)V}{m} \tag{1}$$

The distribution coefficient K_d is a specific value measuring the sorbent's sorption capability listed in Eq. (2).

$$K_d = \frac{(C_0 - C_e)V}{C_e m} \tag{2}$$
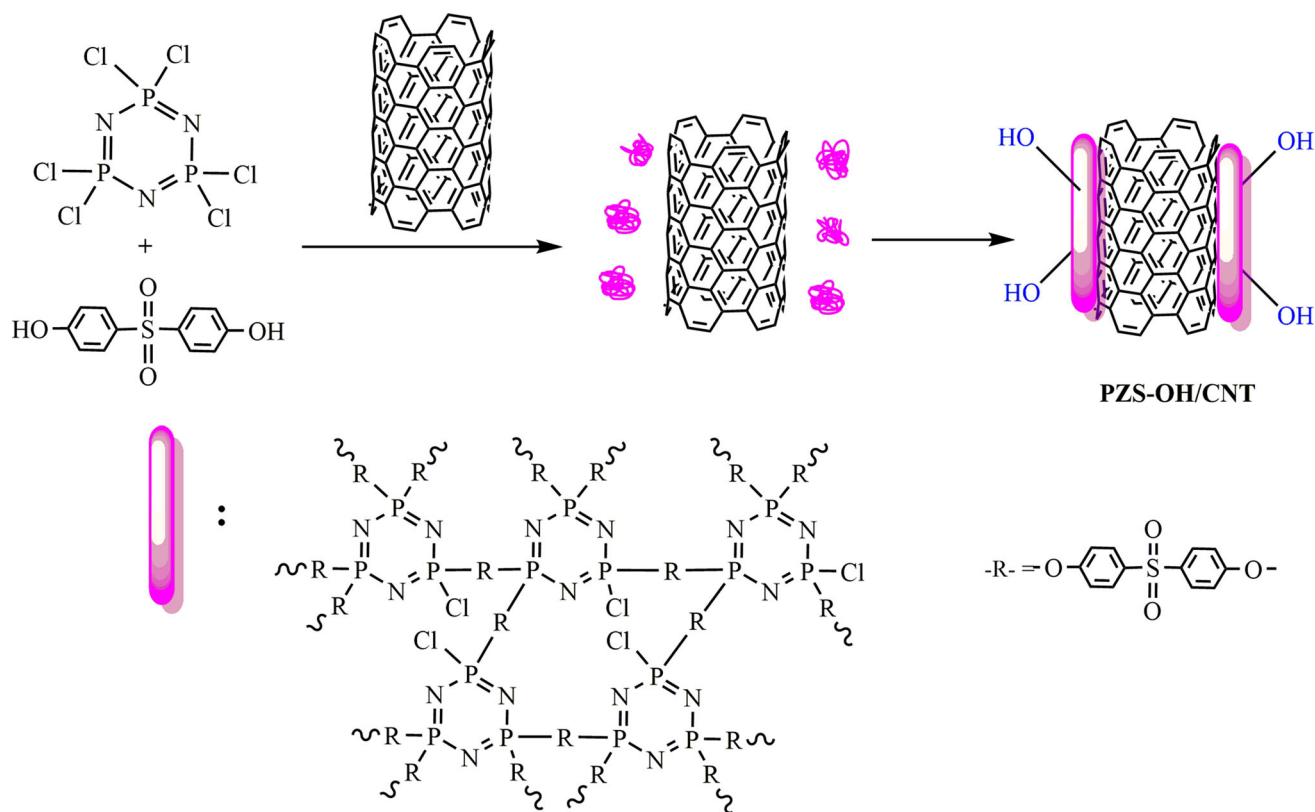
Scheme 1 Synthesis route of PZS-OH/CNT

where C_0 and C_e (mg L^{-1}) is the initial and equilibrium concentrations of U(VI) in the solutions, respectively; V is the volume of the solution (L); m is the mass of dry adsorbents (g).

Results and discussion

Characterization

The FT-IR spectra of CNT, PZS-OH and PZS-OH/CNT were presented in Fig. 1. From the IR spectra of CNTs, it could be observed that the number of functional groups on the surface of CNTs was small, only one broad peak appeared at 1650 ∼ 1900 cm^{-1}, which was assigned to the C–H bending vibration peak. As to the PZS-OH, the adsorption signal at 1140 cm^{-1} orignating from P=N stretching, indicates the presence of phosphazene rings. Two characteristic signals at 1026 and 945 cm^{-1} are attributed to the P–O–C bond. In contrast to PZS-OH/CNT, two continuous peaks appeared at 3000–4000 cm^{-1} and obvious peak at 3400 cm^{-1} was observed which was attributed to the stretching vibration adsorption for –OH. 1268 cm^{-1} was the stretching vibration adsorption peak of C–O, 1164 cm^{-1} was the stretching vibration characteristic
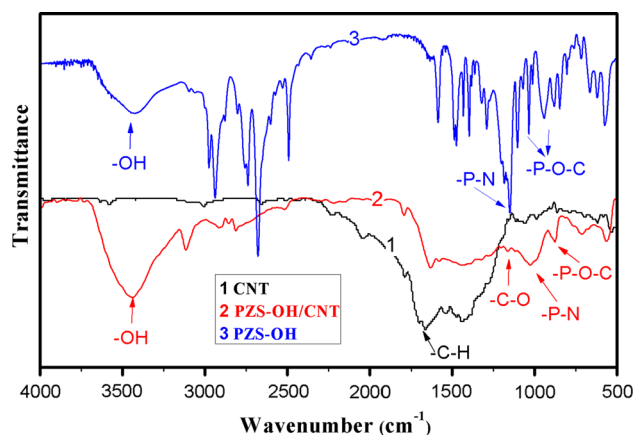

Fig. 1 The FTIR spectra of CNT, PZS-OH and PZS-OH/CNT

absorption peak for C–O–C, and the peak at 750 ∼ 1000 cm^{-1} was the vibration peak for P–N and P–O–C. The results of FT-IR indicated that PZS-OH/CNT has been successfully synthesized.

The SEM images of PZS-OH/CNT and CNT are shown in Fig. 2. As seen from Fig. 2a, CNTs showed a disordered fibrous network consisting of bundled, inter-wined structure while the surface of PZS-OH showed a rough surface (Fig. 2b). The core–shell nanostructure with CNT as the center and PZS-OH layer as the shell could be observed in
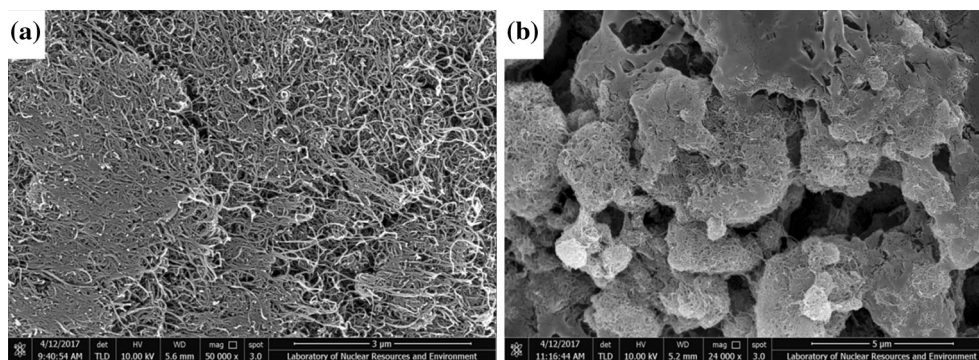
Fig. 2 SEM images of CNT and PZS-OH/CNT

Table 1 BET surface area and pore volume of CNTs and PZS-OH/CNT materials

Materials	S_{BET} (m^2 g^{-1})	V_{pore} (cm^3 g^{-1})	D_A (nm)
CNTs	137.93	0.76	17.49
PZS-OH	18.47	0.04	9.31
PZS-OH/CNT	119.72	0.60	16.47

Fig. 2b. Undoubtedly, PZS-OH chains immobilized onto the surface of CNT.

As pore structure and surface area always influence the performance of adsorption behavior so the N$_2$ adsorption–desorption isothermal characterization is necessary [18, 19]. BET specific surface area (S_{BET}), pore volume (V_{pore}) and Average pore diameter (D_A) of the materials were measured and the results were summarized in Table 1. The lower surface area and pore volume of PZS-OH/CNT, compared with CNTs, indicate that the presence of PZS-OH layer blocked or filled up gaps between the CNTs as well as partially clogged the nanotube openings [20–23].

The XPS spectra of PZS-OH/CNT and CNTs were shown in Fig. 3. A comparison with the survey spectrum of CNTs revealed a new peak of P$_{2p}$, S$_{2p}$ and N$_{1s}$ at 133.8, 167.2 and 396.5 eV, respectively, in the survey spectra of PZS-OH/CNT, indicating the successful addition of the phosphorus, sulfur and nitrogen element on PZS-OH/CNT surface.

Effect of pH

The adsorption of CNTs before and after modification is greatly affected by the pH value, because the pH value affects uranium speciation in the solution, the surface charge of the material and the surface metal binding sites. The adsorption of uranium on CNTs before and after modification was observed under the conditions of pH values between 2 and 7. As shown in Fig. 4, the influence
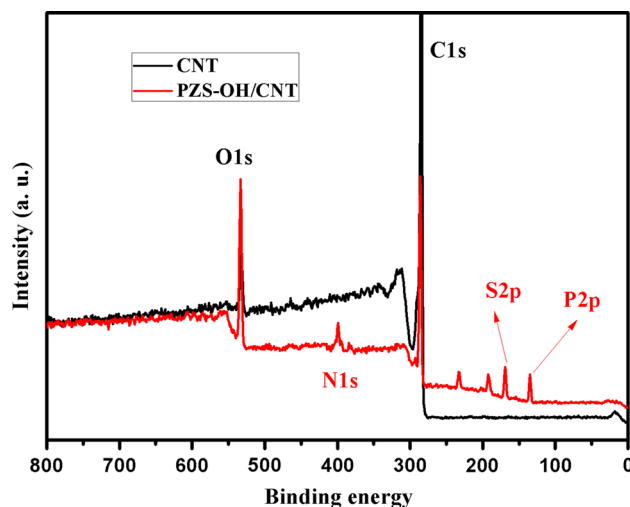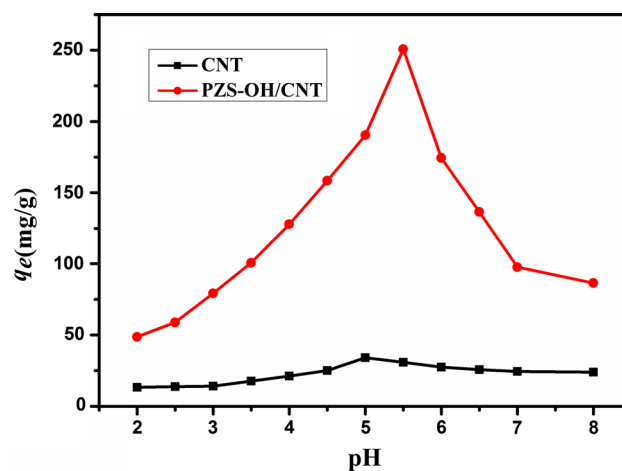

Fig. 3 The XPS spectra of CNT and PZS-OH/CNT

Fig. 4 The effect of initial solution pH on adsorption of U(VI) by CNT and PZS-OH/CNT ($T = 298$ K, $m = 0.01$ g, $C_0 = 100$ mg L^{-1} and $V = 25$ mL)

of uranium adsorption to pH values between CNTs and PZS-OH/CNT were similar. With the increase of pH values, the adsorption capacity first increased and then

decreased. But comparing these two materials, the adsorption capacity of PZS-OH/CNT was stronger than that of CNTs. When the pH was 2, both the pristine and modified CNTs had low adsorption capacity for uranium. This was because that when the pH value was low, the solution contained a lot of H_3O^+ which occupied the surface of the adsorbent. The number of adsorption sites decreased and the adsorption capacity decreased either.

With the increase of pH value, the adsorption capacity of uranium adsorbent increased gradually. When the pH value was 5 and 5.5, respectively, the adsorption capacity of uranium for CNTs and PZS-OH/CNT were the largest, which were 34.14 and 250.79 mg g^{-1}, respectively. When the pH value further increased, the adsorption capacity gradually decreased. This is because that at low pH uranium was in the form of UO_2^{2+}, with the increase of pH value, the concentration of CO_3^{2-}, HCO_3^- ions in solution increased, and uranium can form stable complexes which reduced the adsorption capacity of the adsorbents. This phenomenon illustrated that different forms of uranyl ions which existed in different pH value had an important effects on the adsorption capacity. The optimal pH value for the adsorption of uranium was 5 and 5.5, before and after modification, respectively, and the following experiment will use this value. Figure 5 showed the distribution of uranium species as a function of pH produced using Medusa program. It could be observed that uranium was hydrolyzed in forms of UO_2^{2+}, $UO_2(OH)^+$, $UO_2(OH)_2^{2+}$, $(UO_2)_3(OH)_5^+$ and UO_2CO_3 (aq) at pH < 5.5 [24]. When the pH was higher than 5.5, the low adsorption affinity anion $(UO_2)_3(OH)_7^-$, $UO_2(CO_3)_2^{2-}$ and $UO_2(CO_3)_3^{4-}$ increased, leading the decrease of U(VI) uptake [25].

To achieve a better understanding on the effect of pH for the U(VI) removal, the zeta potentials of the PZS-OH/CNT and CNTs as a function of pH values were shown in Fig. 6. The results indicated that the negative charges increased with the increasing pH for both samples, but PZS-OH/CNT exhibited more negative throughout the pH range compared to CNTs which was attributed to the ionization of –OH group. Furthermore, the point of zero change of PZS-OH (pH$_{PZC}$) was 4.0, which meant when the pH was higher than 4.0, the surface of PZS-OH would be negatively charged. This would facilitate the binding of the positively charged U(VI) cations with negative PZS-OH surface [28], resulting in increased U(VI) adsorption.

Effect of contact time

The influence of contact time of CNTs and PZS-OH/CNT on the adsorption of U(VI) was shown in Fig. 7. It could be observed that the adsorption of CNTs and PZS-OH/CNT of U(VI) increased gradually with the increasing time and reached the adsorption equilibrium at 30 min. At the initial
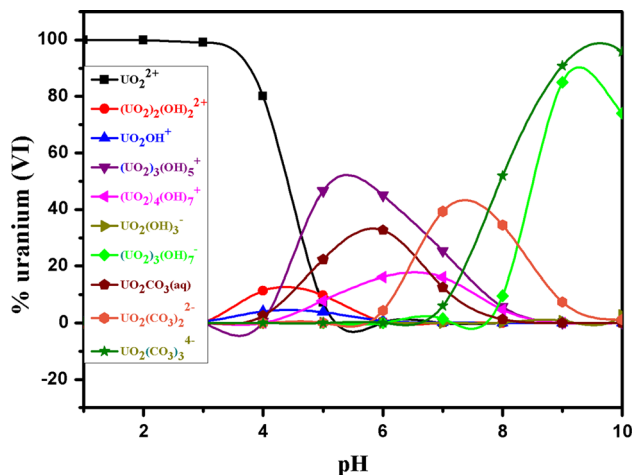

Fig. 5 Distribution of U (VI) species in aqueous solution with a total concentration of 100 mg L^{-1} and pH values ranging from 1 to 10 (calculated by using a Medusa program)
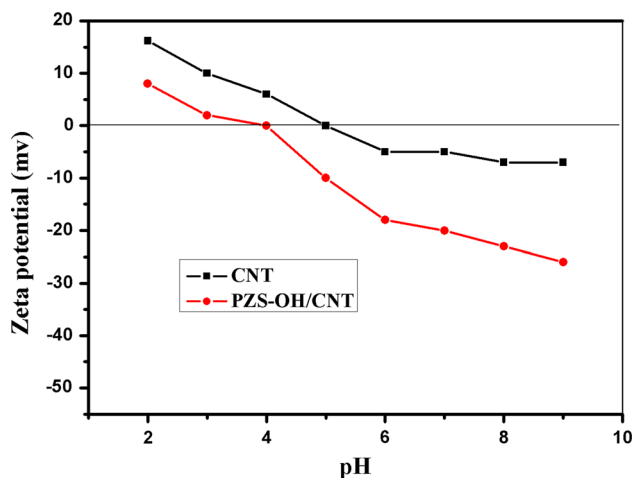

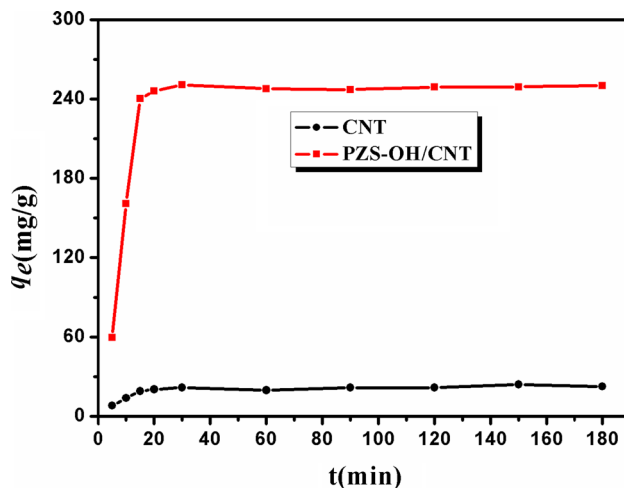**Fig. 6** The zeta potential of PZS-OH/CNT and CNT

Fig. 7 The effect of contact time on adsorption of U(VI) by CNT and PZS-OH/CNT ($T = 298$ K, $m = 0.01$ g, $C_0 = 100$ mg L^{-1} and $V = 25$ mL; CNT: pH 5; PZS-OH/CNT: pH 5.5)

stage of adsorption, the adsorption of U(VI) increased rapidly. This is because that at the beginning, the concentration of uranium was the largest which possesses larger driving force for adsorption. With the concentration of uranium and surface adsorption sites of CNTs decreased continuously, the force of adsorption decreased which made the quantity of adsorption gradually stable. In contrast it could be seen that PZS-OH/CNT on the adsorption of U(VI) was much higher than CNTs. After surface modification, PZS-OH/CNT has a larger number of hydroxyl groups, and the active sites for adsorbing U(VI) increased, resulted into higher adsorption.

In order to investigate the adsorption dynamics, two different kinetic models, pseudo-first-order and pseudo-second-order were used to fit the adsorption process [26]:

The pseudo-first-order model is given as follows:

$$\ln(q_e - q_t) = \ln q_e - k_1 t \qquad (3)$$

The pseudo-second-order model is given as follows:

$$\frac{t}{q_t} = \frac{1}{k_2 q_e^2} + \frac{1}{q_e} t \qquad (4)$$

where q_e and q_t are the amounts of U(VI) adsorbed (mg g^{-1}) at equilibrium and at time (t), respectively, t is the contact time (min), and k_1, k_2 are the rate constants for pseudo-first-order kinetic (min^{-1}), pseudo-second-order kinetic (mg^{-1} min^{-1}), respectively.

The plot of $\ln(q_e - q_t)$ versus t and t/q_t versus t yield linear relationships were shown in Fig. 8a and b. The results were summarized in Table 2. From Fig. 8, it could be observed that the correlation coefficients of pseudo-second order kinetics R^2 (0.9945 and 0.9932, respectively) were better than pseudo-first order kinetics R^2, all higher than 0.99. From Table 2, it could be found that the corresponding theoretical amounts adsorbed U(VI) at equilibrium ($q_{2,cal}$) on CNT and PZS-OH/CNT were 23.70 and 258.4 mg g^{-1}, respectively, which were close to the experimental values ($q_{e,exp}$) 24.08 and 250.59 mg g^{-1}, respectively. So the adsorption of U(VI) on CNT and PZS-OH/CNT are fitted the pseudo-second order kinetic equation very well [27], showing that the rate of adsorption are controlled by chemical adsorption.

Effect of initial concentrations

The effects of the initial U(VI) concentration on CNT and PZS-OH/CNT were investigated under the conditions of pH value of 5, 5.5, respectively, varying from 25 to 150 mg L^{-1}. As observed from Fig. 9, with the increasing of the initial U(VI) concentration, the adsorption capacity
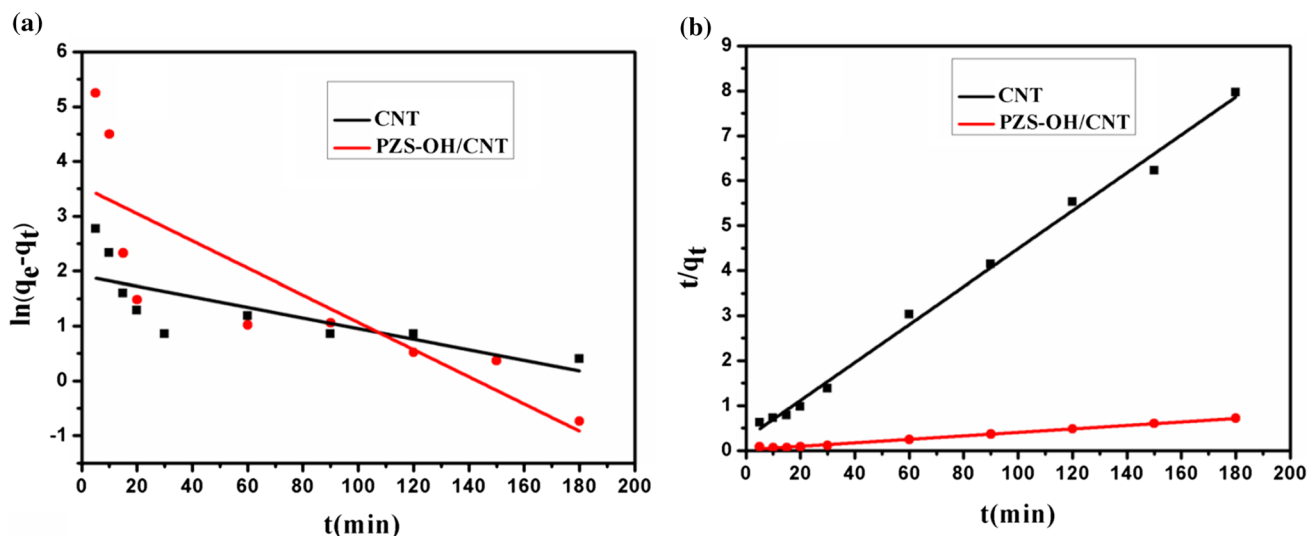

Fig. 8 **a** Pseudo-first-order and **b** pseudo-second-order adsorption kinetics of U(VI) by CNT and PZS-OH/CNT

Table 2 Kinetic parameters for adsorption of U(VI) by CNT and PZS-OH/CNT

Materials	$q_{e,exp}$ (mg g^{-1})	Pseudo-first-order model			Pseudo-second-order model		
		$q_{1,cal}$ (mg g^{-1})	k_1 (min^{-1})	R^2	$q_{2,cal}$ (mg g^{-1})	k_2 (g mg^{-1} min^{-1})	R^2
CNT	24.08	6.82	9.7×10^{-3}	0.514	23.70	6.57×10^{-2}	0.9945
PZS-OH/CNT	250.59	34.64	2.4×10^{-2}	0.650	258.4	8.27×10^{-4}	0.9934

of CNTs before and after modification gradually increased. This may be attributed to high initial concentrations of U(VI) solution, and the concentration gradient between adsorbents/solution interface was greater, which caused the higher equilibrium uptake [25]. When the initial concentration of U(VI) reached 130 mg L^{-1}, the adsorption reached equilibrium. The results showed that the adsorption capacity of PZS-OH/CNT was better than CNTs.

In order to investigate the adsorption behavior of PZS-OH/CNT and CNTs, the Langmuir (Eq. 5) and Freundlich (Eq. 6) isotherms, have been adopted to model sorption isotherms. The linear forms of these two isotherms are expressed as follows:

$$\frac{C_e}{q_e} = \frac{1}{q_m K_L} + \frac{C_e}{q_m} \tag{5}$$

$$\ln q_e = \ln K_F + \frac{1}{n} \ln C_e \tag{6}$$

where q_e is the equilibrium uptake (mg g^{-1}), q_m is the capacity of saturation theory (mg g^{-1}), K_L is the Langmuir adsorption equilibrium constant (L/mg), C_e is the equilibrium concentration (mg L^{-1}), K_F and n are the Freundlich constants related to the adsorption amount and adsorption intensity of the sorbent, respectively.

Linear plots of $\log q_e$ versus $\log C_e$ based on the equilibrium data were given in Fig. 10 and the detailed data were presented in Table 3. The value of the correlation coefficient (R^2) of Langmuir equation was 0.991 and 0.996 for CNTs and PZS-OH/CNT, respectively, higher than the Freundlich model, which meant that the Langmuir model was more fitted the data. From calculated q_m, it could be found that the adsorption capacity of PZS-OH/CNT increased from 41.48 to 338.98 mg g^{-1}, which indicated that the CNTs coated with hydroxyl-polyphosphazene functional groups could greatly improved the adsorption capacity of U(VI).
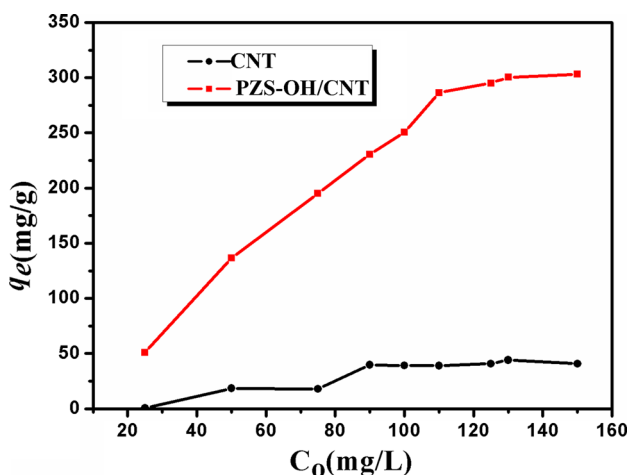

Fig. 9 The effect of initial concentrations on adsorption of U(VI) by CNT and PZS-OH/CNT ($T = 298$ K, $m = 0.01$ g and $V = 25$ mL; CNT: pH 5; PZS-OH/CNT: pH 5.5)

Table 3 Parameters of Langmuir and Freundlich isotherm for adsorption of U(VI) by CNT and PZS-OH/CNT

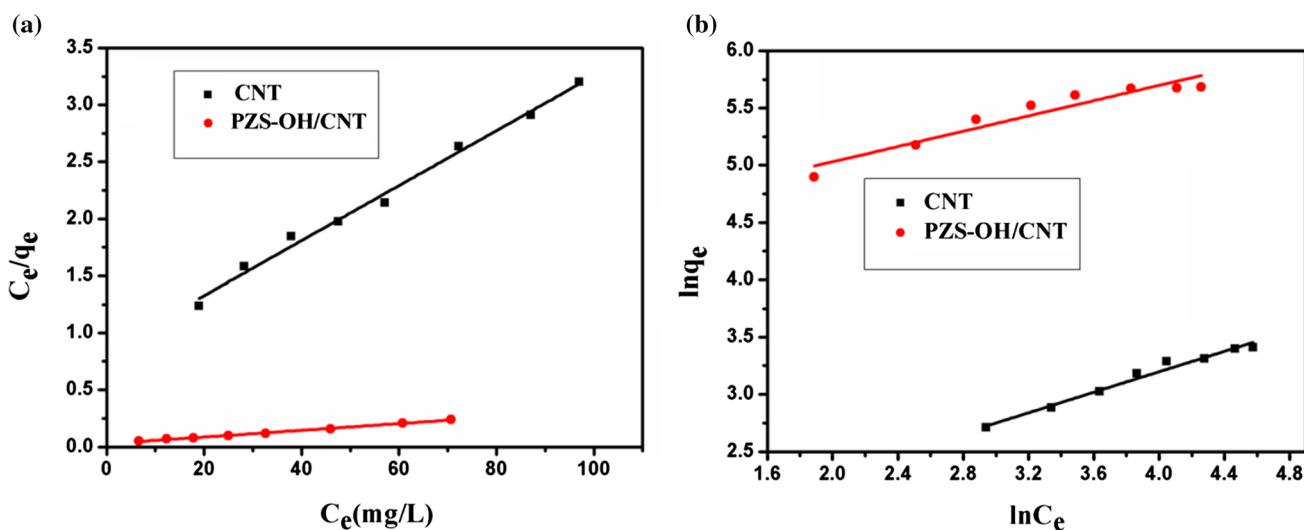| Materials	Langmuir isotherm			Freundlich isotherm		
	K_L	q_m (mg g^{-1})	R^2	K_F	n	R^2
CNT	0.029	41.48	0.991	4.092	2.24	0.975
PZS-OH/CNT	0.105	338.98	0.996	78.51	3.00	0.906

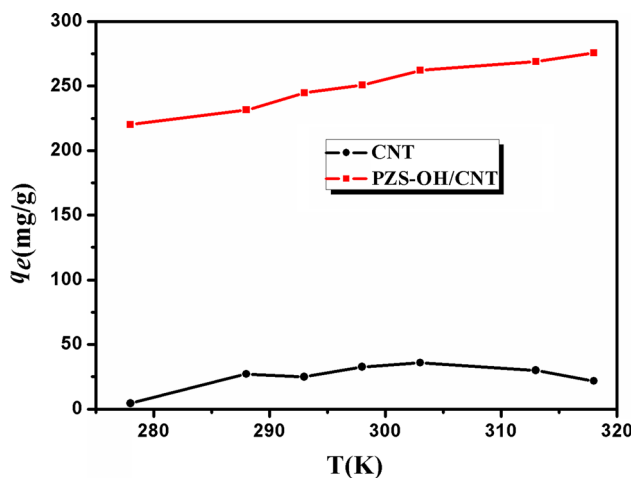Fig. 10 a Langmuir and b Freundlich isotherms of U(VI) adsorbed by CNT and PZS-OH/CNT at 298 K

Fig. 11 The effect of temperatures on adsorption of U(VI) by CNT and PZS-OH/CNT ($m = 0.01$ g, $V = 25$ mL and $C_0 = 130$ mg L^{-1}; CNT: pH 5; PZS-OH/CNT: pH 5.5)
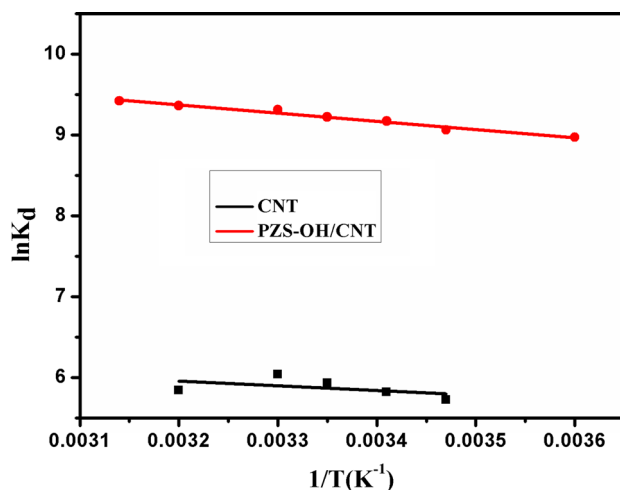
Adsorption thermodynamics

The thermodynamics of adsorption is very important to sorption mechanism as well as kinetics. The effects of temperature on the adsorption of U(VI) by CNTs and PZS-OH/CNT were shown in Fig. 11. It could be found that the adsorption amount of U(VI) increased slowly with the increasing temperature, indicating this was endothermic process, Thus, increasing temperature was conducive to the adsorption process.

The thermodynamic parameters ΔH and ΔS were calculated from the slopes and intercepts for the linear variation of $\ln K_d$ versus $1/T$ by Eq. (7) as shown in Fig. 12. The change of Gibbs free energy ΔG values is acquired by the Eq. (8).

$$\ln K_d = \frac{\Delta S}{R} - \frac{\Delta H}{RT} \tag{7}$$

$$\Delta G = \Delta H - T\Delta S \tag{8}$$

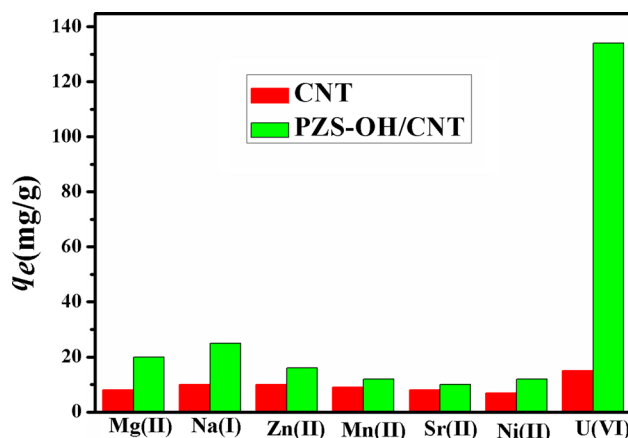**Fig. 12** The thermodynamics for U(VI) adsorption by CNT and PZS-OH/CNT

Fig. 13 Selective sorption capacity of coexistent ions (pH 5.0 for CNTs and pH 5.5 for PZS-OH/CNT, $C_0 = 100$ mg L^{-1}, $V = 25$ mL, $m = 0.01$ g and $T = 298.15$ K)

Table 4 The thermodynamic parameters for U(VI) adsorbed by CNTs and PZS-OH/CNT

Materials	ΔH (kJ mol^{-1})	ΔS (J mol^{-1} K^{-1})	ΔG (kJ mol^{-1})			
			283.15 (K)	288.15 (K)	293.15 (K)	298.15 (K)
CNTs	7.32	72.97	-13.34	-13.71	-14.07	-14.44
PZS-OH/CNT	8.47	104.97	-21.25	-21.78	-22.30	-22.83

Materials	ΔG (kJ mol^{-1})			
	303.15 (K)	308.15 (K)	313.15 (K)	318.15 (K)
CNTs	-14.80	-15.17	-15.53	-15.90
PZS-OH/CNT	-23.35	-23.88	-24.40	-24.93

where K_d is the equilibrium distribution coefficient, ΔH (J mol^{-1}), ΔS (J mol^{-1} K^{-1}) and ΔG (J mol^{-1}) are the enthalpy, entropy and Gibbs free energy, respectively, R (8.314 J mol^{-1} K^{-1}) is the ideal gas constant and T (K) is the thermodynamic Kelvin temperature.

The values of thermodynamic parameters for the adsorption of ΔH, ΔS and ΔG calculated are listed in Table 4, respectively. The positive values of ΔH and ΔS indicated that the adsorption process on PZS-OH/CNT and CNTs was endothermic in nature and the randomness was entropy-driven processes. The values of ΔG between 283.15 and 318.15 K were negative, showing the adsorption on CNTs and PZS-OH/CNT were spontaneous and feasible. With the increase in temperature the values of ΔG decreased, indicated that the adsorption process was more efficient at higher temperatures. The absolute value of ΔG for PZS-OH/CNT was higher than CNTs at the same temperature illustrated that adsorption process for PZS-OH/CNT was more feasible than CNTs.

Selective sorption

In order to evaluate the selectivity of PZS-OH/CNT and CNT for uranium, coexisting ions such as Mg(II), Na(I), Zn(II), Mn(II), Ni(II), Sr(II) and Hg(II) were added into the aqueous solution at the optimal conditions. As shown in Fig. 13, after chemical modification the capacity of U(VI) adsorbed by PZS-OH/CNT was much higher than the coexisting ions, strongly suggesting the selectivity of PZS-OH/CNT was outstanding for U(VI) ions.

Possible sorption mechanism

In order to explore the possible sorption mechanism between U(VI) and PZS-OH/CNT, the XPS spectra of
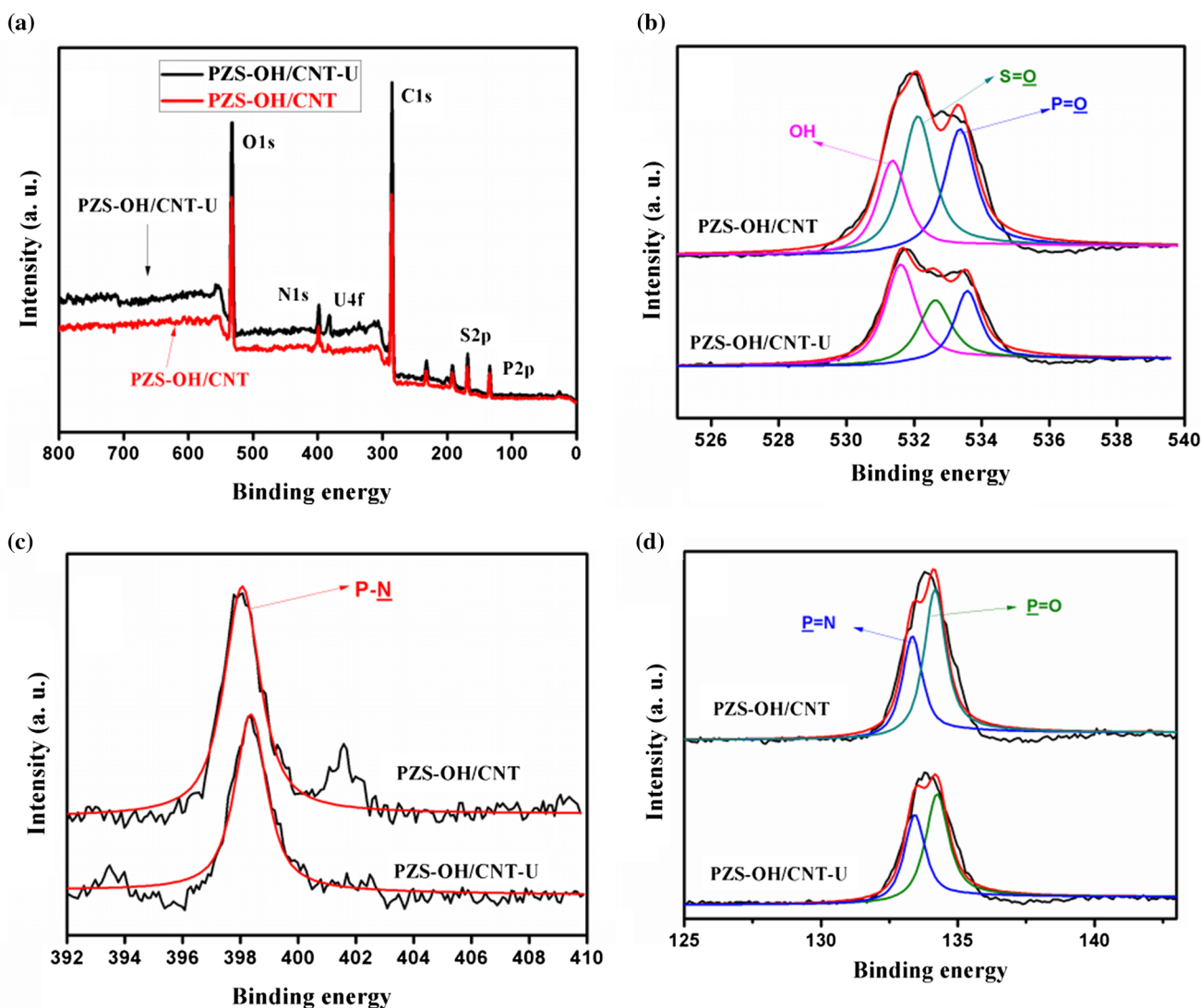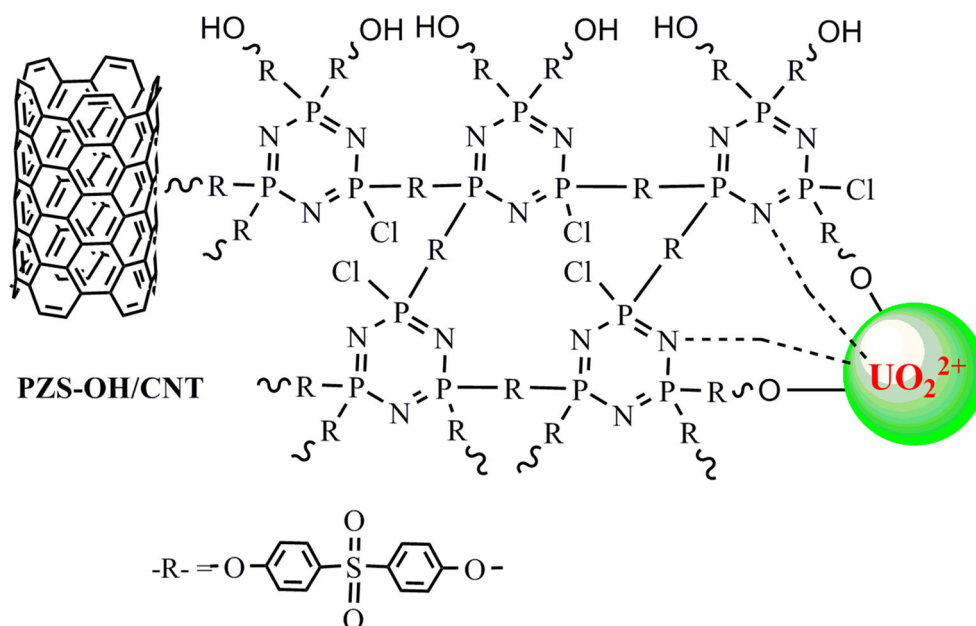

Fig. 14 The typical XPS survey spectra of PZS-OH/CNT (**a**) and PZS-OH/CNT-U (**b**)

Scheme 2 Probable sorption mechanism of U(VI) on PZS-OH/CNT

survey and high resolution scans for O_{1s}, N_{1s} and P_{2p} of the PZS-OH/CNT before and after adsorption were recorded in Fig. 14. It can be found in Fig. 14a that a strong peak in response to U_{4f} peak was in the profile of PZS-OH/CNT-U, which illustrated that U(VI) has been adsorbed onto the surface of PZS-OH/CNT. The O_{1s} spectra can be resolved into three main peaks which can be assigned to S=$\underline{O}$, P=$\underline{O}$ and terminal OH (Fig. 14b). It could be found that the position of OH was shifted to higher binding energy (from 531.0 to 531.4 eV), which the binding energy of S=O (532.3 eV) and P=$\underline{O}$ (533.3 eV) remained unchanged after adsorption. The signal at around 400 eV, in the N_{1s} spectra (Fig. 14c), corresponds to the nitrogen atoms in the phosphazene ring [29]. It was found that the position of N_{1s} was shifted to higher binding energy (from 398.1 to 398.4 eV), indicating the decrease in electron density for the N atoms. As to P_{2p}, the signal was presented around at 133.4 and 134.8 eV due to the phosphorus atoms in the phosphazene ring and $\underline{P}$–O groups, respectively, and they remained unchanged after adsorption (Fig. 14d).

The possible interaction mechanism between U(VI) and PZS-OH/CNT was described in Scheme 2, where U(VI) was coordinated with nitrogen atoms and hydroxyl oxygen atoms.

Conclusions

In this study, PZS-OH/CNT was used to remove U(VI) from aqueous solutions. Effects of pH, contact time, temperature and coexisted ions on the adsorption behavior of the adsorbent were investigated and the results showed that

PZS-ON/CNT has the maximum adsorption capacity of 338.98 mg g^{-1}. Kinetic and thermodynamic studies suggested the sorption process was fast, endothermic and spontaneous. The sorption process obeyed pseudo-second-order model and Langmuir isotherm. The results illustrated that PZS-OH/CNT could be promising candidate as a high selectivity adsorbent for U(VI) removal from aqueous solutions.

References

1. Sun YB, Yang SB, Chen Y, Ding CC, Cheng WC, Wang XK (2015) Adsorption and desorption of U(VI) on functionalized graphene oxides: a combined experimental and theoretical study. Environ Sci Technol 49:4255–4262
2. Pan N, Li L, Ding J, Li SK, Wang RB, Jin YD, Wang XK, Xia CQ (2016) Preparation of graphene oxide-manganese dioxide for highly efficient adsorption and separation of Th(IV)/U(VI). J Hazard Mater 309:107–115
3. Ding DX, Xin X, Li L, Hu N, Li GY, Wang YD, Fu PK (2014) Removal and recovery of U(VI) from low concentration radioactive wastewater by ethylenediamine-modified biomass of aspergillus niger. Water Air Soil Pollut 225(12):1–16
4. Liu SJ, Li S, Zhang HX, Wu LP, Sun L, Ma JG (2016) Removal of uranium(VI) from aqueous solution using graphene oxide and its amine-functionalized composite. J Radioanal Nucl Chem 309:607–614

5. Gao MW, Zhu GR, Wang XH, Wang P, Gao CJ (2015) Preparation of short channels SBA-15-PVC membrane and its adsorption properties for removal of uranium(VI). J Radioanal Nucl Chem 304:675–682

6. Asai S, Limbeck A (2015) LA-ICP-MS of rare earth elements concentrated in cation-exchange resin particles for origin attribution of uranium ore concentrate. Talanta 135:41–49

7. Ohashi Y, Harada M, Asanuma N, Ikeda Y (2015) Feasibility studies on electrochemical recovery of uranium from solid wastes contaminated with uranium using 1-butyl-3-methylimidazorium chloride as an electrolyte. J Nucl Mater 464:119–127

8. Bayramoglu G, Arica MY (2016) MCM-41 silica particles grafted with polyacrylonitrile: modification into amidoxime and carboxyl groups for enhanced uranium removal from aqueous medium. Micropor Mesopor Mat 226:117–124

9. Xiong GX, Liu YH, Cao XH, Zhang ZB, Zhou ZW (2015) Removal of thorium(IV) from aqueous solutions by carboxyl-rich hydrothermal carbon spheres through low-temperature heat treatment in air. Desalin Water Treat 54:2516–2529

10. Singha Deb AK, Ali SM, Shenoy KT (2015) Unanticipated favoured adsorption affinity of Th(IV) ions towards bidentate carboxylate functionalized carbon nanotubes (CNT–COOH) over tridentate diglycolamic acid functionalized CNT: density functional theoretical investigation. RSC Adv 5:80076–80088

11. Tan LC, Liu Q, Jing XY, Liu JY, Song DL, Hu SX, Liu LH, Wang J (2015) Removal of uranium(VI) ions from aqueous solution by magnetic cobalt ferrite/multiwalled carbon nanotubes composites. Chem Eng J 273:307–315

12. Zhao ZW, Li JX, Wen T, Shen CC, Wang XK, Xu AW (2015) Surface functionalization graphene oxide by polydopamine for high affinity of radionuclides. Colloid Surfaces A 482:258–266

13. Fu JW, Wang MH, Wang ST, Wang XZ, Wang HF, Hu L, Xu Q (2011) Supercritical carbon dioxide-assisted preparation of palladium nanoparticles on cyclotriphosphazene-containing polymer nanospheres. Appl Surf Sci 257:7129–7133

14. Elif O, Bunyemin C, Serkan Y (2014) Synthesis and properties of fullerene (C60) substituted cyclophosphazene derivatives. Inorg Chem Commun 49:1–4

15. Xia L, Xia YG, Liu ZP (2015) A novel fluorocyclophosphazene as bifunctional additive for safer lithium-ion batteries. J Power Sour 278:190–196

16. Huang XB, Wei W, Zhao XL, Tang XZ (2010) Novel preparation of polyphosphazene-coated carbon nanotubes as a Pt catalyst support. Chem Commun 46:8848–8850

17. Savvin SB (1961) Analytical use of arsenazo III: determination of thorium, zirconium, uranium and rare earth elements. Talanta 8:673–685

18. Li RM, Che R, Liu Q, Su SZ, Li ZS, Zhang HS, Liu JY, Liu LH, Wang J (2017) Hierarchically structured layered-double-hydroxides derived by ZIF-67 for uranium recovery from simulated seawater. J Hazard Mater 338:167–176

19. Maleki A, Hamesadeghi U, Daraei H, Hayati B, Najafi F, McKay G, Rezaee R (2017) Amine functionalized multi-walled carbon nanotubes: single and binary systems for high capacity dye removal. Chem Eng J 313:826–835

20. Li ZY, Gao B, Chen ZG, Mokaya R, Sotriopoulos S, Puma GL (2011) Carbon nanotube/titanium dioxide (CNT/TiO2) core–shell nanocomposites with tailored shell thickness, CNT content and photocatalytic/photoelectrocatalytic properties. Appl Catal B-Environ 110:50–57

21. Sun WL, Xia J, Shan YC (2014) Comparison kinetics studies of Cu(II) adsorption by multi-walled carbon nanotubes in homo and heterogeneous systems: effect of nano-SiO2. Chem Eng J 250:119–127

22. Thommes M, Kaneko K, Neimark AV, Olivier JP, Rodriguez-Reinoso F, Rouquerol J, Sing KSW (2015) Physisorption of gases, with special reference to the evaluation of surface area and pore size distribution (IUPAC Technical Report). Pure Appl Chem 87:1051–1069

23. Al Hamouz OCS, Adelabu IO, Saleh TA (2017) Novel cross-linked melamine based polyamine/CNT composites for lead ions removal. J Environ Manag 192:163–170

24. Yuan DZ, Chen L, Xiong X, Yuan LG, Liao SJ, Wang Y (2016) Removal of uranium (VI) from aqueous solution by amidoxime functionalized superparamagnetic polymer microspheres prepared by a controlled radical polymerization in the presence of DPE. Chem Eng J 285:358–367

25. Yu SL, Dai Y, Cao XH, Zhang ZB, Liu YH, Ma HJ, Xiao SJ, Lai ZJ, Chen HJ, Zheng ZY, Le ZG (2016) Adsorption of uranium(VI) from aqueous solution using a novel magnetic hydrothermal cross-linking chitosan. J Radioanal Nucl Chem 310:651–660

26. Yuan DZ, Chen L, Xiong X, Zhang QH, Liao SJ, Yuan LG, Wang Y (2016) Synthesis of PAMAM dendron functionalized superparamagnetic polymer microspheres for highly efficient sorption of uranium(VI). J Radioanal Nucl Chem 309:1227–1240

27. Chai K, Ji H (2012) Dual functional adsorption of benzoic acid from wastewater by biological-based chitosan grafted β-cyclodextrin. Chem Eng J 203:309–318

28. Liu X, Li JX, Wang XX, Chen CL, Wang XK (2015) High performance of phosphate-functionalized graphene oxide for the selective adsorption of U(VI) from acidic solution. J Nucl Mater 466:56–64

29. Liang WJ, Zhao B, Zhao PH, Zhang CY, Liu YQ (2017) Bisphenol-S bridged penta(anilino)cyclotriphosphazene and its application in epoxy resins: synthesis, thermal degradation, and flame retardancy. Polym Degrad Stab 135:140–151